Pushwinder Kumar[1*], *Satya Bir Singh*[2**], *Sarvesh Kumar Jain*[3]

CREEP BEHAVIOUR OF ISOTROPIC PRESSURE VESSEL WITH HEMISPHERICAL ENDS SUBJECTED TO INTERNAL PRESSURE

PUZANJE KOD IZOTROPNE POSUDE POD PRITISKOM SA POLUSFERNIM DANCEM POD DEJSTVOM UNUTRAŠNJEG PRITISKA

Originalni naučni rad / Original scientific paper
Rad primljen / Paper received: 26.09.2024
https://doi.org/10.69644/ivk-2025-01-0111

Adresa autora / Author's address:
[1)] Department of Applied Sciences, Chandigarh Engineering College, CGC, Landran, Mohali, Punjab, India
[*]email: pushwindershelly@gmail.com
[2)] Department of Mathematics, Punjabi University, Patiala, Punjab, India, [**]email: sbsingh69@yahoo.com
S.B. Singh https://orcid.org/0000-0003-1381-4903
[3)] Department of Civil Engineering, Madhav Institute of Technology and Science, Gwalior, Madya Pradesh, India
S.K. Jain https://orcid.org/0000-0003-2527-6030

Keywords
- modelling
- pressure vessel
- hemispherical ends
- threshold creep law
- creep

Abstract

Pressure vessels are such type of engineering structure commonly used in many aspects in many industries such as aerospace industry, transport industry for transfer of fuels, nuclear reactors. In this paper we analyse the creep behaviour of an isotropic pressure vessel with hemispherical ends made of Al-SiC$_p$ composite subjected to internal pressure and establish a mathematical model for the pressure vessel with hemispherical ends as a modular structure made of two parts: first part is the middle portion of the vessel as a cylinder subjected to internal pressure; and the second part as hemispherical ends of the pressure vessel subjected to internal pressure. We analyse the effect of reinforcement size (P = 1.7 μm, 14.5 μm, and 45.9 μm) on the creep behaviour and strength of pressure vessel. Threshold creep law has been used for this analysis, because due to apparently high activation energy and high stress exponent, Norton's law is not preferable. We conclude that the creep rates for cylindrical and spherical parts of the pressure vessel composed of composite material with 1.7 μm size of reinforcement as compared with other cases with reinforcement sizes of 14.7 μm and 45.9 μm, show highly reliable character of the structure. This concludes that the structure with reinforcement size of 1.7 μm is highly reliable for the design.

Ključne reči
- modeliranje
- posuda pod pritiskom
- polusferna danca
- zakon dopuštenog napona puzanja
- puzanje

Izvod

Posude pod pritiskom su takav tip inženjerske konstrukcije koje se često koriste u mnogim aspektima industrija, kao što su aerokosmička, industrija transporta za transport goriva, nuklearni reaktori. U ovom radu analiziramo ponašanje puzanja izotropne posude pod pritiskom sa polusfernim dancem od Al-SiC$_p$ kompozita, koja je opterećena unutrašnjim pritiskom, i definišemo matematički model za posudu pod pritiskom sa polusfernim dancem kao modularnu konstrukciju sastavljenu iz dva dela: prvi deo je srednji cilindrični deo posude pod dejstvom unutrašnjeg pritiska; a drugi deo su polusferna danca posude opterećena unutrašnjim pritiskom. Dajemo analizu uticaja veličine čestičnog ojačanja (P = 1,7 μm, 14,5 μm i 45,9 μm) na ponašanje puzanja i čvrstoću posude. Za analizu je primenjen zakon dopuštenog napona puzanja, jer je Nortonov zakon neprikladan zbog evidentno velike aktivacione energije i velikog eksponenta napona. Zaključujemo da brzine puzanja cilindričnog i sfernih delova posude pod pritiskom od kompozitnog materijala sa čestičnim ojačanjem 1,7 μm, pokazuju mnogo veću pouzdanost u ponašanju konstrukcije u odnosu na ostale slučajeve veličine ojačanja od 14,7 μm i 45,9 μm. Time zaključujemo da je konstrukcija izvedena kompozitom sa veličinom čestičnog ojačanja 1,7 μm vrlo pouzdana u projektovanju.

INTRODUCTION

Pressure vessels composed of composite materials offer significant advantages over traditional materials like steel or aluminium. The main causes of these benefits are composite materials' high strength, low weight, and resistance to corrosion, /1-3/. Pressure vessels are very common structures used in different ways in many industries. Spacecraft, satellites, and launch vehicles are among the aerospace applications that use composite pressure vessels. Their lightweight design makes them perfect for holding gases such as propellants, pressurised air, or other fluids, as it minimises the overall weight and fuel consumption of vehicles. Composite pressure vessels are used in the automobile sector to store hydrogen or compressed natural gas (CNG) for fuel cell vehicles. The internal pressure is distributed more evenly over the whole surface of the pressure vessel with hemispherical ends. In comparison to pressure vessels with flat ends, this leads to smaller stress concentration, reducing the possibility of structural collapse. Spherical ends are naturally sturdy and resilient to pressure from both the inside and the outside due to their curvature. Because of its strength, pressure vessels with hemispherical ends have improved structural integrity and can tolerate high pressures. Vessels with flat or dished ends typically have sharp corners and transitions; spherical ends eliminate this. The lack of stress concentration spots at junctions lowers the possibility of fatigue and increases the vessel's overall durability. We consider the pressure vessel with hemispherical ends subjected to internal pressure and we establish a mathematical model for the pressure vessel with hemispherical ends as modular structure made of two parts: first part is the mid portion of the vessel as a cylinder subjected to internal pressure; and the second part are hemispherical ends of the pressure vessel subjected to internal pressure. The performance and behaviour of a structure can be greatly influenced by the size and volume content of the reinforcement, especially in reinforced concrete structures. This parameter is essential for figuring out the structure's strength, durability, structural integrity, and other characteristics. Strength and load-bearing capability of a structure are generally improved by increasing the volume content of the reinforcement. The amount of reinforcement present in a structure can affect its shear and flexural properties. In order to avoid excessive deflection, cracking and shear failure, enough reinforcing is necessary. In recent times many researchers have studied creep behaviour of pressure vessels. Primary creep analysis of an anisotropic thick-walled spherical shell under internal pressure was investigated by Bhatnagar et al. /4/. Miller /5/ evaluated solutions for stresses and displacements in a thick spherical shell subjected to internal and external pressure. You et al. /6/ presented a highly precise model to carry out elastic analysis of thick-walled spherical pressure vessels. Nejad et al. /7/ studied creep stresses in isotropic and homogeneous thick-walled spherical pressure vessels under internal and external pressure and discussed the creep response of the material using Norton's law and the effect of changes in material properties on the stresses and displacement. Bhatnagar and Arya /8/ evaluated creep behaviour of thick-walled cylinder considering large strains using finite strain theory. Bhatnagar et al. /9/ studied creep analysis of thick-walled orthotropic rotating cylinder using finite strain theory to examine the effect of anisotropy on strain rate and stresses. Creep deformation for internally pressurised spherical and cylindrical vessels also was done by some researchers in recent times /10-12/. Singh and Gupta /13/ studied the effect of content, size and reinforcement, and operating temperature on the strain rate and stresses in Al-SiC$_p$ composite cylinder considering the internal pressure using threshold creep law and observing a significant variation in stresses and strain rate with variation in the size and content of the reinforcement and operational temperature.

MATHEMATICAL MODEL

The following assumptions are made in the analysis:

- the material is homogeneous and remains isotropic during creep;
- there are no volume changes during creep;
- the total strain is composed of elastic and creep strain components.

Consider an anisotropic pressure vessel made of Al-SiC$_p$ composite with hemispherical ends, with inner radius '*a*' and outer radius '*b*' for the cylindrical part as well as hemispherical ends, subjected to internal pressure '*p*', i.e., following boundary conditions, which implies

at inner radius (*a*),

radial stress $\sigma_r|_{r=a} = -p$, (1)

at outer radius (*b*),

radial stress $\sigma_r|_{r=b} = 0$. (2)

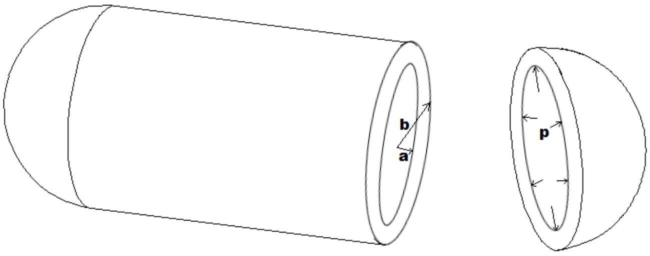

Figure 1. Cross section of pressure vessel with hemispherical ends subjected to internal pressure.

In aluminium matrix composite materials subjected to creep conditions, the effective strain rate is linked with effective stress, with well established threshold stress base law:

$$\dot{\varepsilon} = [M(\sigma - \sigma_0)]^n , \tag{3}$$

where: $\dot{\varepsilon}$, σ, and σ_0 are effective strain rate, effective stress, and threshold stress, respectively.

So effective stress is written as,

$$\sigma = \frac{\dot{\varepsilon}^{1/n}}{M} + \sigma_0 , \tag{4}$$

where: M and σ_0 are known as creep parameters and depend upon the material and application temperature (T). The size of reinforcement and the quantity of reinforcement are important for analysis. Creep parameters have been estimated from creep results reported in literature for Al-SiC$_p$ composite (Singh and Gupta, /14/). The relation between strain rates and displacement rate are given as

$$\dot{\varepsilon}_r = \frac{d\dot{u}}{dr} , \tag{5}$$

$$\dot{\varepsilon}_\theta = \frac{\dot{u}}{r} . \tag{6}$$

Eliminating $\dot{u}$ from the above equations, we get compatibility equation as

$$r\frac{d\dot{\varepsilon}_\theta}{dr} = \dot{\varepsilon}_r - \dot{\varepsilon}_\theta . \tag{7}$$

Now we analyse the pressure vessel with hemispherical ends as two sections. The first one is the cylindrical mid section, the second section are hemispherical sections on both ends of the pressure vessel.

ANALYSIS OF CYLINDRICAL MIDDLE SECTION OF PRESSURE VESSEL

The equilibrium equation for cylinder is given as

$$r\frac{d\sigma_r}{dr} = (\sigma_\theta - \sigma_r) . \tag{8}$$

Assuming there is no change in volume, then the sum of creep strain rates is given as

$$\dot{\varepsilon}_r + \dot{\varepsilon}_\theta + \dot{\varepsilon}_z = 0 . \tag{9}$$

Fundamental constitutive equations for isotropic materials given by Bhatnagar and Gupta /15/ are given as

$$\dot{\varepsilon}_r = \frac{\dot{\varepsilon}}{2\sigma}[2\sigma_r - \sigma_\theta - \sigma_z] , \tag{10}$$

$$\dot{\varepsilon}_\theta = \frac{\dot{\varepsilon}}{2\sigma}[2\sigma_\theta - \sigma_z - \sigma_r] , \tag{11}$$

$$\dot{\varepsilon}_z = \frac{\dot{\varepsilon}}{2\sigma}[2\sigma_z - \sigma_r - \sigma_\theta], \quad (12)$$

where: σ_r, σ_θ, and σ_z are radial, tangential and longitudinal stresses. The structure does not change in volume, therefore plane strain condition is applicable, i.e., longitudinal strain rate is zero, and we get

$$\dot{\varepsilon}_z = 0, \quad (13)$$

$$\sigma_z = \frac{\sigma_r + \sigma_\theta}{2}. \quad (14)$$

Putting the value of the longitudinal stress in Eq.(10) and Eq.(11), we have

$$\dot{\varepsilon}_r = \frac{3\dot{\varepsilon}}{4\sigma}[\sigma_r - \sigma_\theta], \quad (15)$$

$$\dot{\varepsilon}_\theta = \frac{3\dot{\varepsilon}}{4\sigma}[\sigma_\theta - \sigma_r]. \quad (16)$$

The effective stress is given as

$$\sigma = \frac{1}{\sqrt{2}}[(\sigma_\theta - \sigma_z)^2 + (\sigma_z - \sigma_r)^2 + (\sigma_\theta - \sigma_r)^2]^{1/2}. \quad (17)$$

Substituting value of longitudinal stress, we get

$$\sigma = \frac{\sqrt{3}}{2}(\sigma_\theta - \sigma_r). \quad (18)$$

Solving Eq.(15) and Eq.(16) with the help of Eq.(18), we get

$$\dot{\varepsilon} = -\frac{2}{\sqrt{3}}\dot{\varepsilon}_r = \frac{2}{\sqrt{3}}\dot{\varepsilon}_\theta. \quad (19)$$

From Eqs. (7) and (19), we have

$$r\frac{d\dot{\varepsilon}_\theta}{dr} + 2\dot{\varepsilon}_\theta = 0. \quad (20)$$

Separating the variables and integrating the above equation, we get

$$\dot{\varepsilon}_\theta = \frac{C_1}{r^2}. \quad (21)$$

Now putting the value of $\dot{\varepsilon}_\theta$ in Eq.(19), we get effective strain rate as

$$\dot{\varepsilon} = \frac{2}{\sqrt{3}}\dot{\varepsilon}_\theta = \frac{2C_1}{r^2\sqrt{3}}. \quad (22)$$

Now we solve Eq.(8) with the help of Eqs. (4) and (22), we get

$$r\frac{d\sigma_r}{dr} = \frac{2^{\frac{n+1}{n}} C_1^{\frac{1}{n}}}{r^{\frac{2}{n}} 3^{\frac{n+1}{2n}} M} + \frac{2}{\sqrt{3}}\sigma_0 \quad (23)$$

Integrating the above equation and taking limits from inner radius 'a' to radius 'r', we get

$$\sigma_r = \frac{n 2^{\frac{1}{n}} C_1^{\frac{1}{n}}}{3^{\frac{n+1}{2n}} M}\left[r^{-\frac{2}{n}} - a^{-\frac{2}{n}}\right] + \frac{2}{\sqrt{3}}\sigma_0 \ln\left(\frac{r}{a}\right) - p. \quad (24)$$

Now we substitute the boundary condition from Eq.(2), and we get

$$\frac{p + \frac{2}{\sqrt{3}}\sigma_0 \ln\left(\frac{a}{b}\right)}{\left[a^{-\frac{2}{n}} - b^{-\frac{2}{n}}\right]} \frac{3^{\frac{n+1}{2n}} M}{n 2^{\frac{1}{n}}} = C_1^{\frac{1}{n}}. \quad (25)$$

Putting the value of integrating constant and radial stress becomes

$$\sigma_r = -\frac{n 2^{\frac{1}{n}}}{3^{\frac{n+1}{2n}} M}\left[\frac{p + \frac{2}{\sqrt{3}}\sigma_0 \ln\left(\frac{a}{b}\right)}{\left[a^{-\frac{2}{n}} - b^{-\frac{2}{n}}\right]} \frac{3^{\frac{n+1}{2n}} M}{n 2^{\frac{1}{n}}}\right]\left[r^{-\frac{2}{n}} - a^{-\frac{2}{n}}\right] + $$
$$+ \frac{2}{\sqrt{3}}\sigma_0 \ln\left(\frac{r}{a}\right) - p. \quad (26)$$

We rewrite the above equation as

$$\sigma_r = X\left[r^{-\frac{2}{n}} - a^{-\frac{2}{n}}\right] + \frac{2}{\sqrt{3}}\sigma_0 \ln\left(\frac{r}{a}\right) - p, \quad (27)$$

where: X is given as

$$X = \frac{p + \frac{2}{\sqrt{3}}\sigma_0 \ln\left(\frac{a}{b}\right)}{a^{-\frac{2}{n}} - b^{-\frac{2}{n}}}. \quad (28)$$

Also from Eq.(18), we calculate the value of tangential stress as

$$\sigma_\theta = \frac{2}{\sqrt{3}}\sigma + \sigma_r. \quad (29)$$

Radial stresses are calculated from Eq.(27) for particular composite material. From Eq.(29) with the help of effective stress we find out the tangential stress. Also, the longitudinal stress is calculated from Eq.(14) by using radial and tangential stresses. We calculate the effective strain rate as well as radial and tangential strain rates from Eqs. (3) and (19).

ANALYSIS OF HEMISPHERICAL SECTION OF PRESSURE VESSEL

A small element of the hemispherical ends of the pressure vessel is considered in equilibrium of forces in the radial direction and we may write,

$$r\frac{d\sigma_r}{dr} = 2(\sigma_\theta - \sigma_r). \quad (30)$$

Now, constitutive equations of steady state creep in the isotropic material are considered, and due to the spherical symmetry of the spherical vessel, we write, $\sigma_\theta = \sigma_\phi$

$$\dot{\varepsilon}_r = \frac{\dot{\varepsilon}}{\sigma}[\sigma_r - \sigma_\theta], \quad (31)$$

$$\dot{\varepsilon}_\theta = \frac{\dot{\varepsilon}}{2\sigma}[\sigma_\theta - \sigma_r], \quad (32)$$

$$\dot{\varepsilon}_\phi = \frac{\dot{\varepsilon}}{2\sigma}[\sigma_\theta - \sigma_r], \quad (33)$$

where: σ_r, σ_θ, and σ_ϕ are radial, tangential, and longitudinal stresses. The well known Von-Mises yield criterion is

$$\sigma = (\sigma_\theta - \sigma_r). \quad (34)$$

Solving Eqs. (31), (32), and (33) with the help of Eq. (34), we get

$$\dot{\varepsilon} = -\dot{\varepsilon}_r = 2\dot{\varepsilon}_\theta = 2\dot{\varepsilon}_\phi. \quad (35)$$

Using this in Eq.(7), we get

$$r\frac{d\dot{\varepsilon}_\theta}{dr} + 3\dot{\varepsilon}_\theta = 0. \quad (36)$$

Separating the variables and integrating the above equation, we get

$$\dot{\varepsilon}_\theta = \frac{C_1}{r^3}. \quad (37)$$

Now, we put the value of $\dot{\varepsilon}_\theta$ in Eq.(35) and we get the effective strain rate as,

$$\dot{\varepsilon} = 2\dot{\varepsilon}_{\theta} = \frac{2C_1}{r^3}\,. \qquad (38)$$

Now, solving Eq.(30) with the help of Eqs. (4) and (38), we get

$$r\frac{d\sigma_r}{dr} = \frac{2^{\frac{n+1}{n}}\,C_1^{\frac{1}{n}}}{r^{\frac{3}{n}}M} + 2\sigma_0\,. \qquad (39)$$

Integrating the above equation and taking limits from inner radius ‘*a*’ to radius ‘*r*’, we get

$$\sigma_r = -\frac{n}{3}\frac{2^{\frac{n+1}{n}}\,C_1^{\frac{1}{n}}}{M}\left[r^{-\frac{3}{n}} - a^{-\frac{3}{n}}\right] + 2\sigma_0\ln\left(\frac{r}{a}\right) - p\,. \qquad (40)$$

Now, substituting the boundary condition from Eq.(2), we get

$$\frac{p + 2\sigma_0\ln\left(\frac{r}{a}\right)}{\left[a^{-\frac{3}{n}} - b^{-\frac{3}{n}}\right]}\,\frac{3M}{n2^{\frac{n+1}{n}}} = C_1^{\frac{1}{n}}\,. \qquad (41)$$

Putting the value of integrating constant and radial stress becomes,

$$\sigma_r = -\frac{n}{3}\frac{2^{\frac{n+1}{n}}}{M}\,\frac{p + 2\sigma_0\ln\left(\frac{r}{a}\right)}{\left[a^{-\frac{3}{n}} - b^{-\frac{3}{n}}\right]}\,\frac{3M}{n2^{\frac{n+1}{n}}}\left[r^{-\frac{3}{n}} - a^{-\frac{3}{n}}\right] + 2\sigma_0\ln\left(\frac{r}{a}\right) - p \qquad (42)$$

We rewrite the above equation as

$$\sigma_r = Y\left[a^{-\frac{3}{n}} - r^{-\frac{3}{n}}\right] + 2\sigma_0\ln\left(\frac{r}{a}\right) - p\,, \qquad (43)$$

where Y is given as

$$Y = \frac{p + 2\sigma_0\ln\left(\frac{a}{b}\right)}{a^{-\frac{3}{n}} - b^{-\frac{3}{n}}}\,. \qquad (44)$$

Also from Eq.(34), we calculate the value of tangential stress as

$$\sigma_{\theta} = \sigma + \sigma_r\,. \qquad (45)$$

Radial stresses are calculated from Eq.(34), for particular composite material. From Eq.(45) with the help of effective stress we find out the tangential stress. We calculate the effective strain rate as well as the radial and tangential strain rates from Eqs. (3) and (35).

PARAMETERS USED IN THIS STUDY

We consider a pressure vessel made of Al-SiC$_p$ with hemispherical ends subjected to internal pressure. Based on the mathematical solution present above, values of stresses and strain rates are calculated for different combinations reinforcement size. Results are established by considering the following data: inner radius of pressure vessel is 500 mm; outer radius of pressure vessel is 800 mm; internal pressure is 100 MPa.

The creep parameters M and σ_0 required in the calculations are shown in Table 1.

Table 1. Creep parameters for Al-SiC$_p$ composite.

P (μm)	T (°C)	V (vol.%)	M (s$^{-1/5}$MPa)	σ_0 (MPa)	Coefficient of correlation
1.7	350	10	0.00435	19.83	0.945
14.5	350	10	0.00872	16.50	0.999
45.9	350	10	0.00939	16.29	0.998

NUMERICAL RESULTS

Stress distribution at different reinforcement size at 10 % of reinforcement volume

Numerical results from the current analysis for the stress distribution for different reinforcement sizes (P = 1.7 μm, 14.5 μm, and 45.9 μm) at 10 % of reinforcement volume for both cylindrical and spherical parts of an isotropic pressure vessel with hemispherical ends are plotted in Figs. 2 to 4.

The variations in stress magnitude for the three different cases (P = 1.7 μm, 14.5 μm, and 45.9 μm) are clearly not significant. Radial stresses for cylindrical and spherical part of a pressure vessel are similar for all three cases of different reinforcement size and show a compressive nature on the entire radii. Tangential and longitudinal stresses remain tensile in nature on the entire radii for both cylindrical and spherical part of the pressure vessel. The tangential stresses developed in the spherical part are much lower as compared to the cylindrical part of the vessel. Variations in radial and longitudinal stresses are not significant in both cylindrical and the spherical part of the pressure vessel. All three stresses (radial, tangential, and longitudinal) have least magnitude at the inner radius and increase along inner to outer radius.

The effective stress for the cylindrical and spherical parts of the pressure vessel are plotted in Fig. 4. It is clearly seen that effective stresses developed in the spherical part are much lower as compared to the cylindrical part of pressure vessel for all three cases of different reinforcement size.

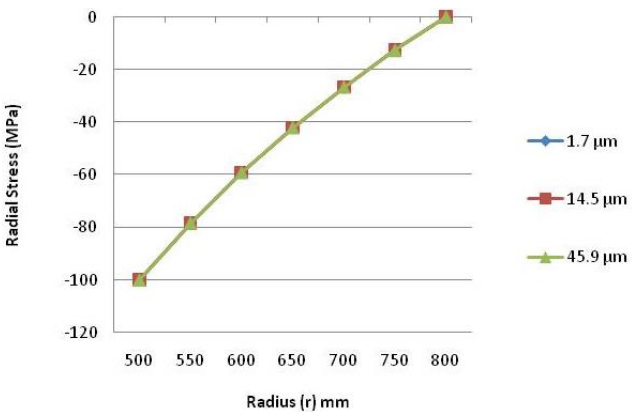

Figure 2a. Variation of radial stress for the cylindrical part of pressure vessel.

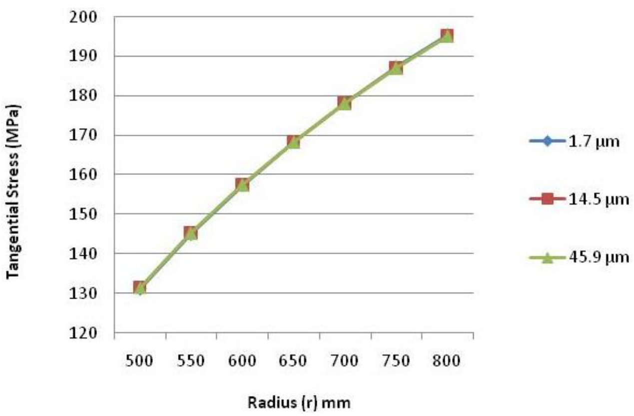

Figure 2b. Variation of tangential stress for the cylindrical part of pressure vessel.

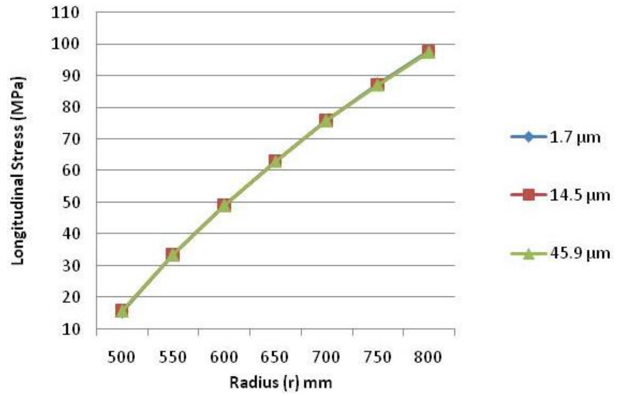

Figure 2c. Variation of longitudinal stress for the cylindrical part of pressure vessel.

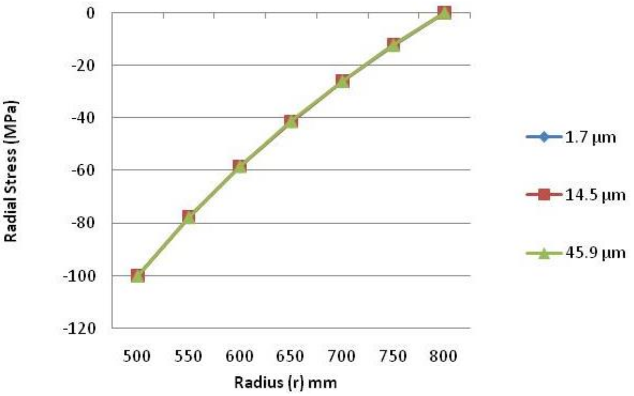

Figure 3a. Variation of radial stress for the spherical part of pressure vessel.

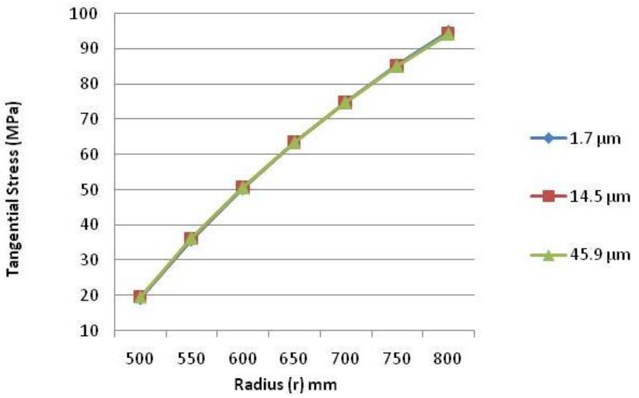

Figure 3b. Variation of tangential stress for the spherical part of pressure vessel.

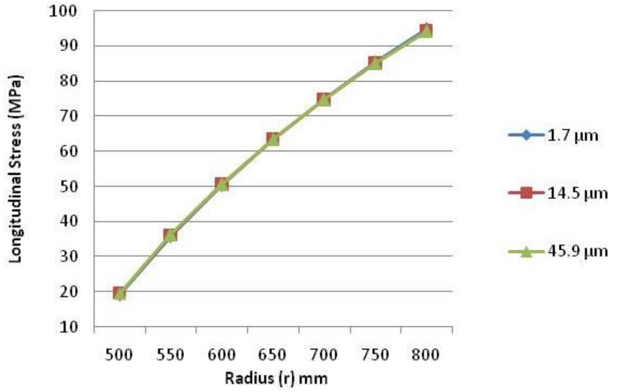

Figure 3c. Variation of longitudinal stress for the spherical part of pressure vessel.

The magnitude of effective stress has maximum value at inner radii and decreases from inner to outer radii.

Effective strain rates are significantly lower when size of reinforcement is taken as 1.7 μm among the three cases of reinforcement size for both cylindrical and spherical part of the pressure vessel.

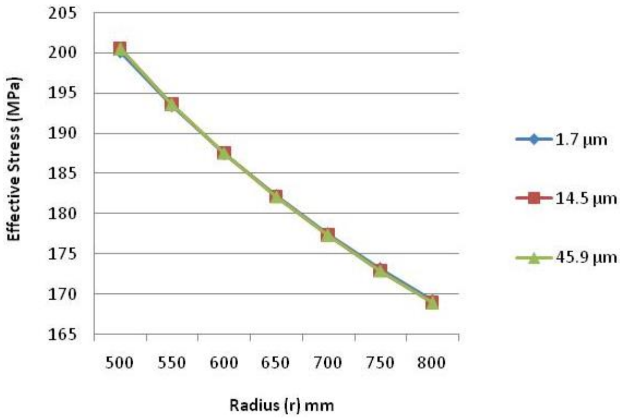

Figure 4a. Variation of effective stresses in the cylindrical part of pressure vessel.

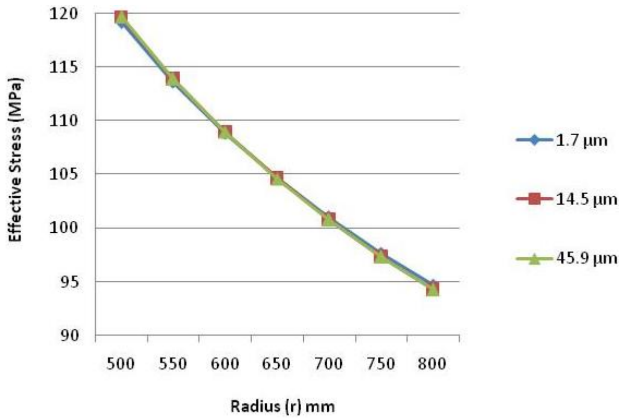

Figure 4b. Variation of effective stresses in the spherical part of pressure vessel.

Creep rates for different reinforcement size at 10 % of reinforcement volume

Creep rates for different reinforcement size for the cylindrical and spherical part of the pressure vessel are plotted in Figs. 5 and 6.

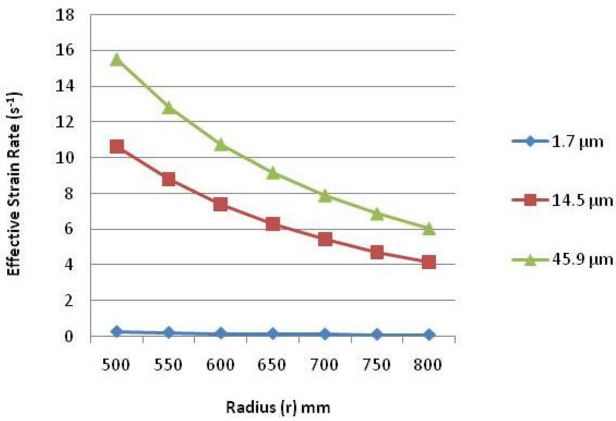

Figure 5a. Variation of effective strain rates for the cylindrical part of pressure vessel.

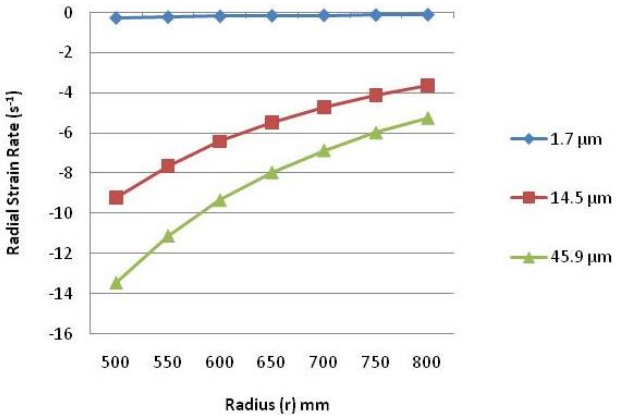

Figure 5b. Variation of radial strain rates for the cylindrical part of pressure vessel.

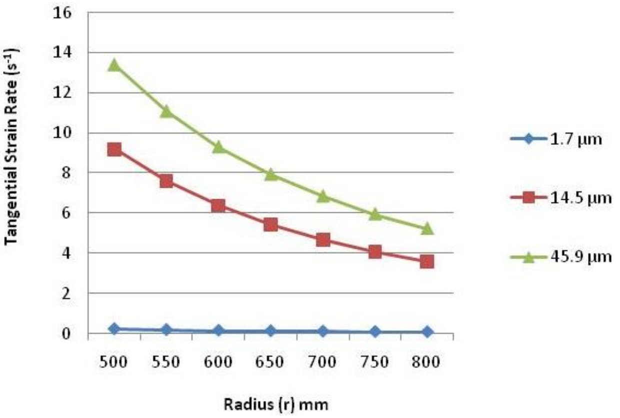

Figure 5c. Variation of tangential strain rates for the cylindrical part of pressure vessel.

In the second case when reinforcement size is taken as 14.5 μm, the effective strain rates are lower as compared to 45.9 μm reinforcement size, but have larger values as compared to 1.7 μm. Similarly, tangential strain rates follow same trends as effective strain rates, but with lower values for all three cases of reinforcement size for both the cylindrical and spherical part of pressure vessel as shown in Figs. 5 and 6.

In the spherical part of pressure vessel effective strain rate and tangential strain rates have positive values and much lower values as compared to the cylindrical part of pressure vessel for all three cases of reinforcement size at 10 % reinforcement volume.

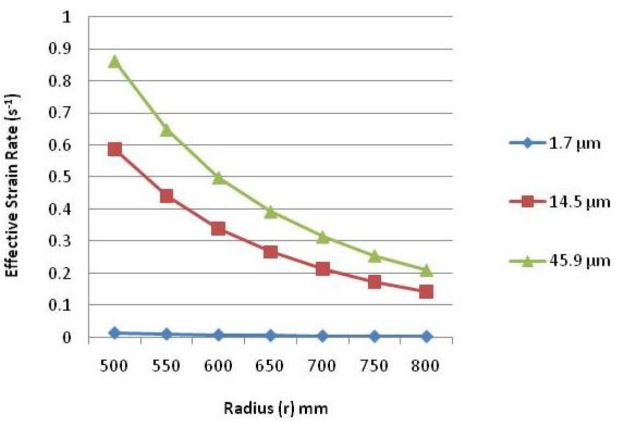

Figure 6a. Variation of effective strain rates for the spherical part of pressure vessel.

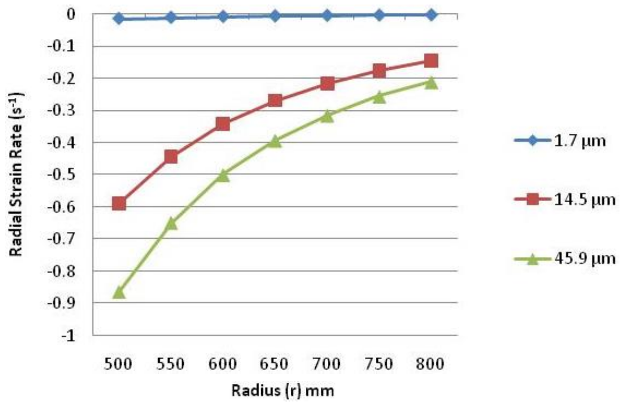

Figure 6b. Variation of radial strain rates for the spherical part of pressure vessel.

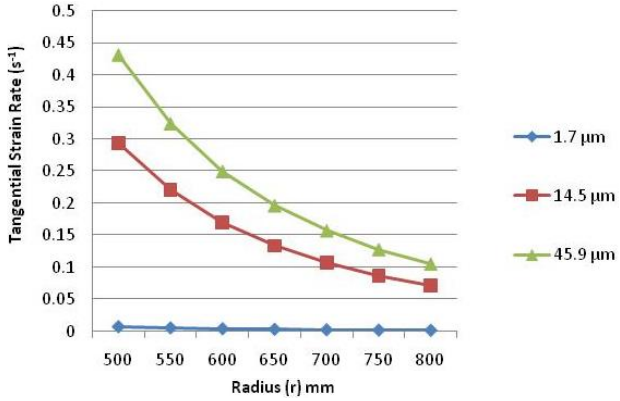

Figure 6c. Variation of tangential strain rates for the spherical part of pressure vessel.

Radial strain rates are negative for both cylindrical and spherical part of pressure vessel. Absolute values of radial strain rates for 1.7 μm reinforcement size are much lower among the three cases of reinforcement size. In the second case when reinforcement size is 14.5 μm the modulus values of radial strain rates are lower as compared to the 45.9 μm reinforcement size but are larger as compared to 1.7 μm for both cylindrical and spherical part of pressure vessel. Among the cylindrical and spherical part, absolute values of radial strain rates are much lower for all three cases of reinforcement size for 10 % volume of reinforcement.

Stress distribution at reinforcement size P = 1.7 μm at 10 % of reinforcement volume

Further, we compare stresses in cylindrical and spherical parts of pressure vessel when reinforcement size is taken as 1.7 μm. Radial stresses do not have a significant difference for cylindrical and spherical parts of the pressure vessel as shown in Fig. 7 and remain compressive in nature throughout the radius. We observe that the tangential stress in the cylindrical part is higher as compared to the spherical part of pressure vessel and has minimal value at inner radii and increases with increase in radius, as shown in Fig. 7, and shows tangential nature throughout the entire radius. Longitudinal stresses in the cylindrical and spherical part of the pressure vessel do not have much significant difference, as seen from Fig. 7. Longitudinal stress has a minimal value at the inner radius as the tangential stress and increases with increase in radius.

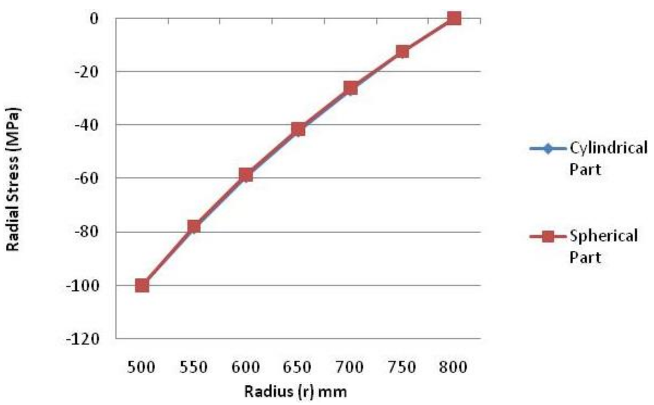

Figure 7a. Variation of radial stress for reinforcement size P = 1.7 μm at 10 % volume for the cylindrical and spherical part of pressure vessel.

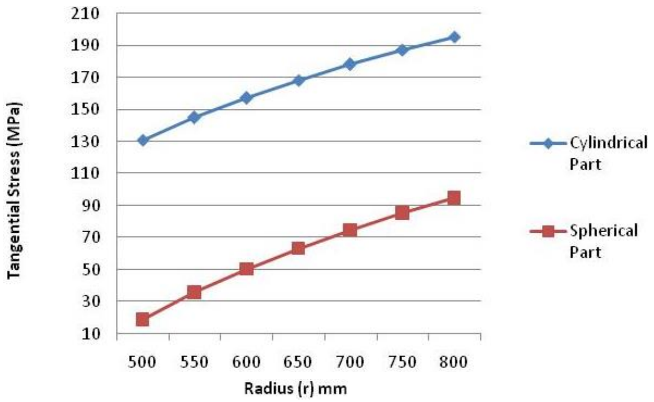

Figure 7b. Variation of tangential stress for reinforcement size P = 1.7 μm at 10 % volume for the cylindrical and spherical part of pressure vessel.

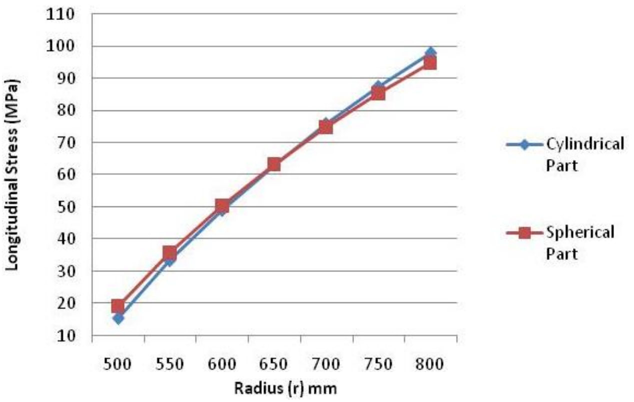

Figure 7c. Variation of longitudinal stress for reinforcement size P = 1.7 μm at 10 % volume for the cylindrical and spherical part of pressure vessel.

Effective stresses have a significant difference for the cylindrical and spherical part of pressure vessel. From Fig. 8 it is observed that effective stresses for the cylindrical part are much higher than for the spherical part of the pressure vessel and shows a tensile nature throughout the entire radii.

Creep rates for reinforcement size P = 1.7 μm at 10 % of reinforcement volume

Creep rates are plotted in Fig. 9 when we consider the size of reinforcement as 1.7 μm at 10 % reinforcement volume.

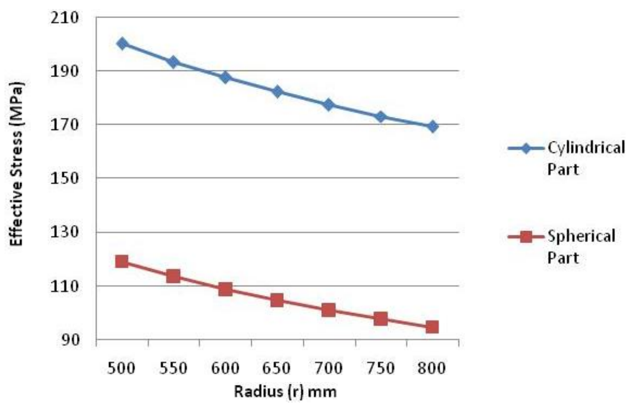

Figure 8. Variation of effective stress for reinforcement size P = 1.7 μm at 10 % volume for the cylindrical and spherical part of pressure vessel.

From Fig. 9 it is observed that in the spherical part the creep rates are significantly lower as compared to the cylindrical part of pressure vessel. Effective strain and tangential strain rate remain positive throughout the entire radii and have a maximal value at the inner radii and decrease when moving from inner to outer radii. The tangential strain rate shows similar trends as compared to effective strain rates but with lower values for both cylindrical and spherical part of the pressure vessel. Radial strain rate remains negative on the entire radii. The absolute value of radial strain rate is much lower in the case of the spherical part of pressure vessel as compared to the cylindrical part.

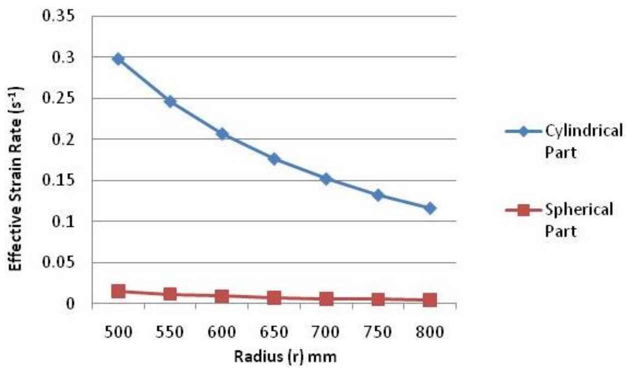

Figure 9a. Variation of effective strain rate for reinforcement size P = 1.7 μm at 10 % volume for the cylindrical and spherical part of pressure vessel.

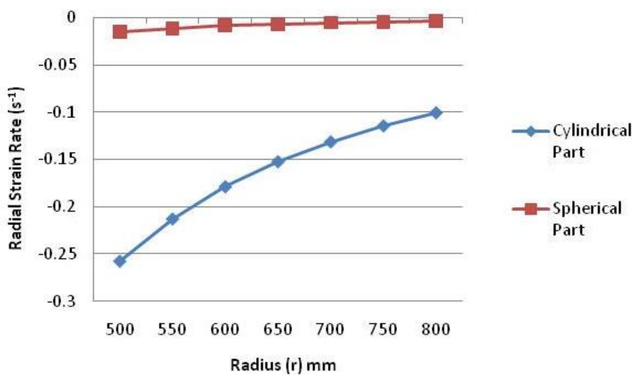

Figure 9b. Variation of radial strain rate for reinforcement size P = 1.7 μm at 10 % volume for the cylindrical and spherical part of pressure vessel.

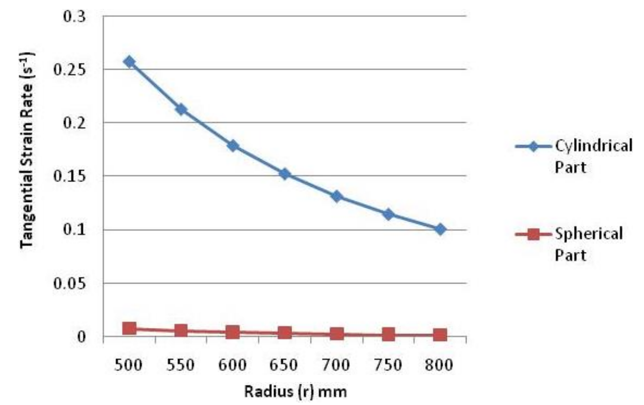

Figure 9c. Variation of tangential strain rate for reinforcement size P = 1.7 μm at 10 % volume for the cylindrical and spherical part of pressure vessel.

Creep rates of cylindrical part at P = 1.7 μm and spherical part at P = 14.5 μm at 10 % of reinforcement volume

From Fig. 9 it is observed that creep rates for cylindrical and spherical part have a significant difference. We compare creep rates for cylindrical part with reinforcement size of 1.7 μm and spherical part of the pressure vessel with reinforcement size of 14.5 μm, as shown in Fig. 10. In this situation the effective strain rate is higher in the spherical part as compared to the cylindrical part of pressure vessel at inner radii, but at outer radii the difference is much less as shown in Fig. 10.

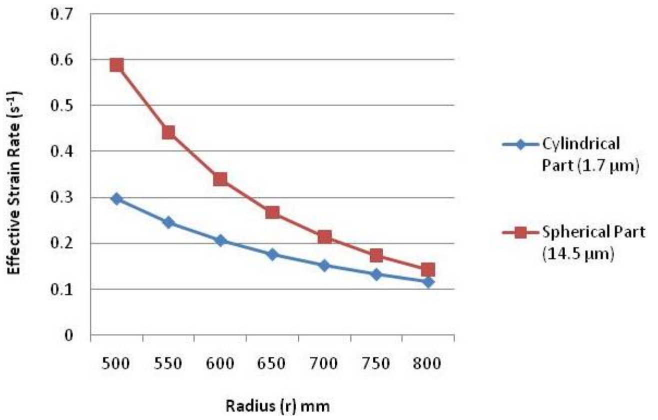

Figure 10a. Variation of effective strain rate for the cylindrical part at P = 1.7 μm and spherical part at P = 14.5 μm at 10 % volume.

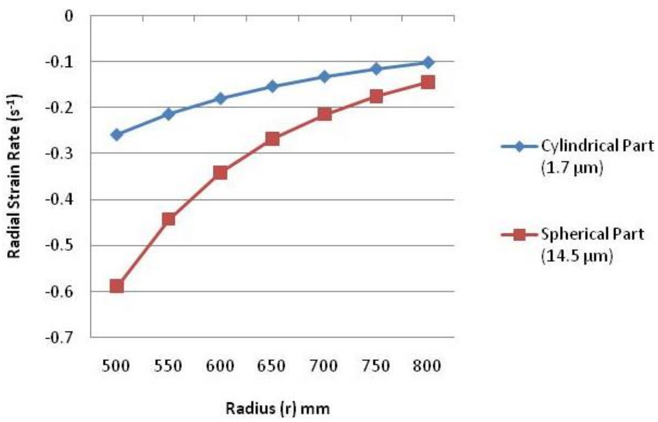

Figure 10b. Variation of radial strain rate for the cylindrical part at P = 1.7 μm and spherical part at P = 14.5 μm at 10 % volume.

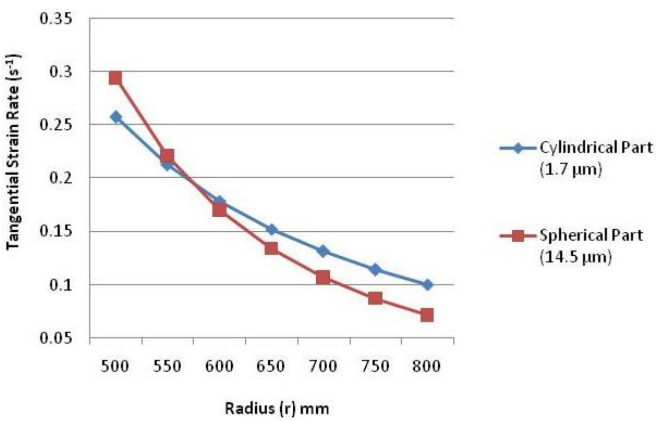

Figure 10c. Variation of tangential strain rate for the cylindrical part at P = 1.7 μm and spherical part at P = 14.5 μm at 10 % volume.

The tangential strain rate at inner radii for the spherical part is higher but when we move from inner to outer radii the tangential strain rate for the cylindrical part is higher, as compared to the spherical part of pressure vessel. Effective and tangential strain rates remain positive throughout the entire radii, tangential strain rates having lower value than effective strain rates for both cylindrical and spherical part of pressure vessel. Radial strain rates are negative for the entire radii. Absolute value of radial strain rate is lower in the case of the cylindrical part as compared to the spherical part of the pressure vessel. At inner radii there is a larger difference between the absolute value of radial strain rate, but at the outer radii the difference is much lesser.

CONCLUSIONS

It is primarily concluded that:

- Stress concentrations for cylindrical and spherical parts of the pressure vessel accumulate at varying radii (500 - 800 mm) with highly similar intensity for different sizes of reinforcement. The effective stresses have maximal intensity/concentration at the internal radius and diminish as we approach the outer radius for all different sizes of the reinforcement. The nonlinear character is visible in the graphs.
- The effective strain rate for cylindrical and spherical parts of the pressure vessel composed of composite material with 1.7 μm reinforcement size is compared with other cases with reinforcement sizes of 14.7 μm and 45.9 μm and shows a highly reliable character of the structure. The strains do not suddenly drop as we approach the outer radius in the case of 1.7 μm reinforcement size compared to the other cases. This concludes that the structure with reinforcement size of 1.7 μm is highly reliable in the design.
- Radial, tangential and effective stresses are much higher in the cylindrical part of the pressure vessel as compared to the spherical part. Also, strain rates are much higher in the cylindrical part as compared to the spherical part of the pressure vessel.

FUTURE SCOPE

We made analysis with 10 % of reinforcement volume. As observed, the cylindrical part has much higher values of stresses and strains as compared to the spherical part of the pressure vessel. We shall increase the reinforcement volume to form/fabricate a structure in which the stresses and strain concentration/distribution are uniform.

REFERENCES

1. Altenbach, H., Altenbach, J., Kissing, W., Mechanics of Composite Structural Elements, 2nd Ed., Springer Nature Singapore Pte Ltd., 2018. doi: 10.1007/978-981-10-8935-0
2. Boyle, J.T., Spence, J., Stress Analysis for Creep, Butterworth & Co. Ltd, 1983.
3. Erdogan, E., Kibler, J.J. (1969), *Cylindrical and spherical shells with cracks*, Int. J Fract. Mech. 5: 229-237. doi: 10.1007/BF00184614
4. Bhatnagar, N.S., Kulkarni, P.S., Ayra, V.K. (1987), *Primary creep analysis of an anisotropic thick-walled spherical shell,* J Press. Ves. Technol. 109(3): 347-351. doi: 10.1115/1.3264876
5. Miller, G.K. (1995), *Stresses in a spherical pressure vessel undergoing creep and dimensional changes*, Int. J Solids Struct. 32(14): 2077-2093. doi: 10.1016/0020-7683(94)00197-5
6. You, Z., Buttlar, W.G. (2005), *Application of discrete element modeling techniques to predict complex modulus of asphalt-aggregate hollow cylinders subjected to internal pressure*, J Transp. Res. Board, 1929(1): 218-226. doi: 10.1177/0361198105192900126
7. Nejad, M.Z., Hoseini, Z., Niknejad, A., Ghannad, M. (2011), *A new analytical solution for creep stresses in thick-walled spherical pressure vessels*, J Basic Appl. Sci. Res. 1(11): 2162-2166.
8. Bhatnagar, N.S., Arya, V.K. (1974), *Large strain creep analysis of thick-walled cylinder*, Int. J Non-Linear Mech. 9(2): 127-140. doi: 10.1016/0020-7462(74)90004-3
9. Bhatnagar, N.S., Kulkarni, P.S., Ayra, V.K. (1986), *Creep analysis of orthotropic rotating cylinders considering finite strain*, Int. J Non-Linear Mech. 21(1): 61-71. doi: 10.1016/0020-7462(86)90013-2
10. Temesgen, A.G., Singh, S.B., Pankaj, T. (2022), *Modeling of creep deformation in an internally pressurized transversely isotropic spherical shell subjected to a thermal gradient*, Mech. Solids, 57(4): 937-948. doi: 10.3103/S0025654422040185
11. Li, Y.Z., Fu, J.W., Qian, L.F., Wang, H.Y. (2023), *On the discussions of nonlinear terms in the large deformation model of thin-walled cylindrical shells*, Mech. Solids, 58(4): 1214-1227. doi: 10.3103/S0025654423600216
12. Verma, G., Thakur, P. (2022), *Comparative creep analysis of spherical shell made up of different materials*, Mech. Solids, 57(5): 1214-1221. doi: 10.3103/S0025654422050120
13. Gupta, V.K., Singh, S.B., Ray, S. (2009), *Role of reinforcement geometry on the steady state creep behavior of a rotating composite disc*, Multidisc. Model. Mater. Struct. 5(2): 139-150. doi: 10.1163/157361109787959840
14. Singh, T., Gupta, V.K. (2009), *Effect of material parameters on steady state creep in a thick composite cylinder subjected to internal pressure*, J Eng. Res. 6(2): 20-32. doi: 10.24200/tjer.vol6iss2pp20-32
15. Bhatnagar, N.S., Gupta, R.P. (1966), *On the constitutive equations of the orthotropic theory of creep*, J Phys. Soc. Japan, 21(5): 1003-1007. doi: 10.1143/JPSJ.21.1003